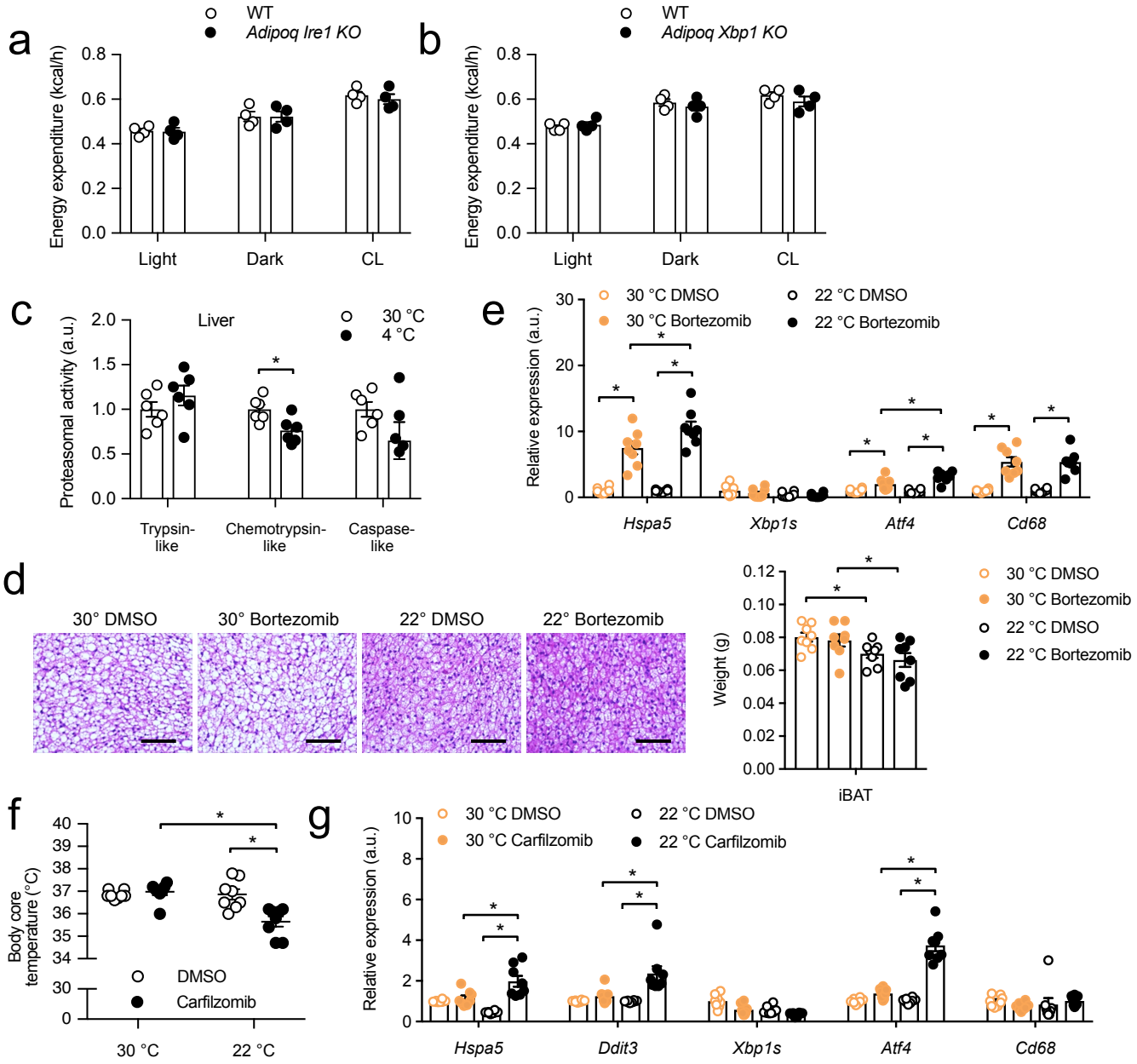

Supplementary Fig. 1 Role of UPR and UPS in BAT for ER homeostasis. (**a,b**) Whole body energy expenditure during light phase, dark phase or during CL316,243 (CL) stimulation in mice lacking Ire1α or Xbp1 in adipocytes (Biol. replicates n=4, **P*<0.05 by T-Test). (**c**) Proteasome activity in livers from wild-type (WT) mice after 7 days of adaptation to 4 °C or 30 °C (biol. replicates n=6, **P*<0.05 by T-Test). (**d**) Representative H&E histology as well as tissue weights of interscapular brown adipose tissue (iBAT) from WT mice housed at 22 °C or 30 °C 16 h after Bortezomib (2.5 mg/kg) or control DMSO treatment (Biol. replicates n=8, **P*<0.05 by 2-way ANOVA, Scale bar: 100 µm) (**e**) mRNA levels of stress markers in the livers of WT mice housed at 22 °C or 30 °C 16 h after Bortezomib (2.5 mg/kg) or control DMSO treatment (Biol. replicates n=8, normalized to ΔCT, **P*<0.05 by 2-way ANOVA). (**f**) Body core temperature after 4 h carfilzomib (4 mg/kg) or control DMSO treatment in WT mice housed at 22 °C or 30 °C (Biol. replicates n=8, **P*<0.05 by 2-way ANOVA). (**g**) mRNA levels of stress markers in BAT of WT mice housed at 22 °C or 30 °C after 6 h carfilzomib (4 mg/kg) or control DMSO treatment in (Biol. replicates n=8, normalized by ΔCT, **P*<0.05 by 2-way ANOVA).

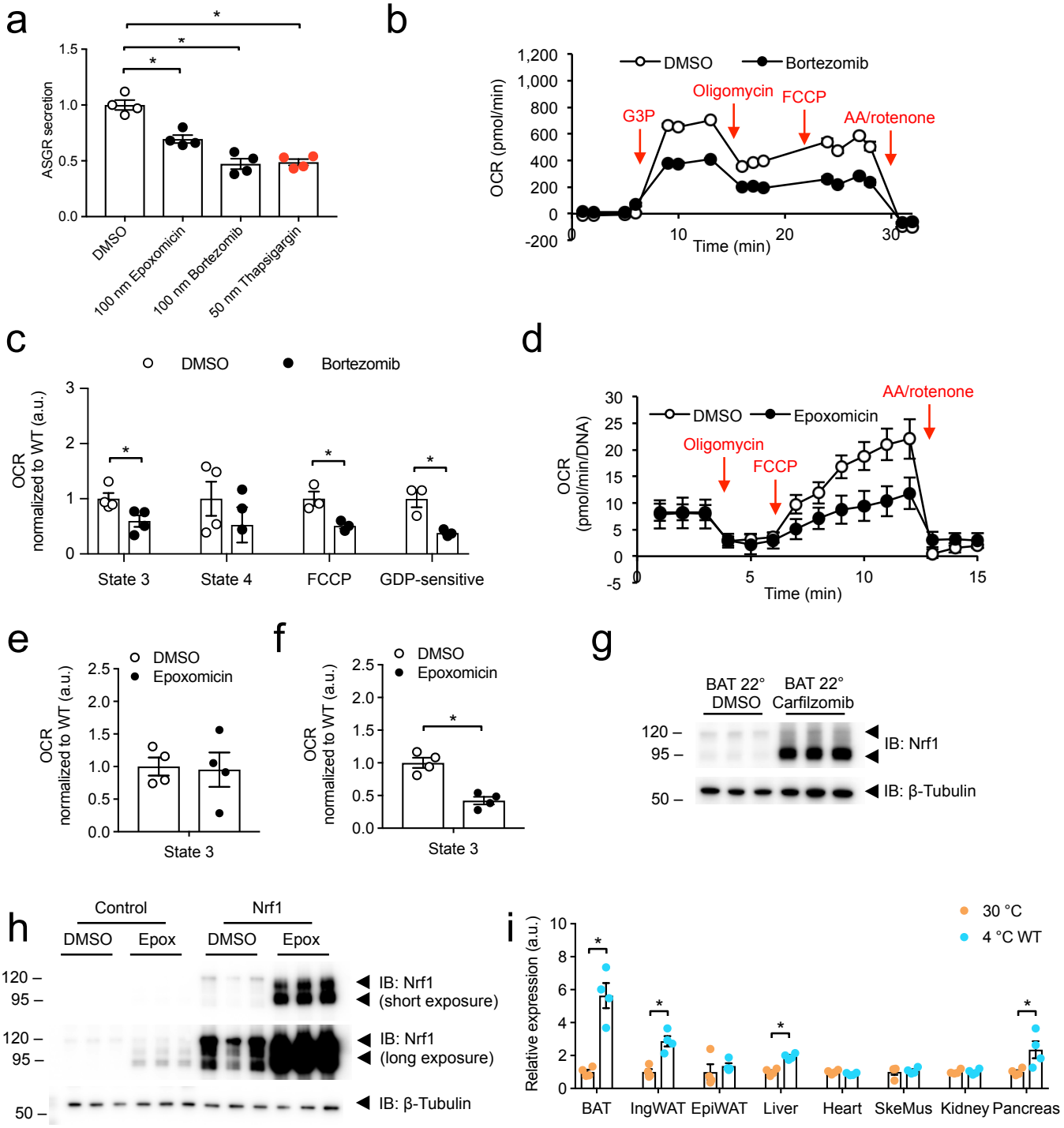

Supplementary Fig. 2 Proteasomal activity is required for mitochondrial respiration. (**a**) ER functional reporter assay measuring asialoglycoprotein receptor (ASGR) secretion in control, epoxomicin, bortezomib or thapsigargin treated 3T3-L1 adipocytes (Tech. replicates n=4, **P*<0.05 by 1-way ANOVA). (**b**) Oxygen consumption rate (OCR) in mitochondria isolated from BAT of WT mice 16 h after bortezomib (2.5 mg/kg) or DMSO at 22 °C (representative traces) (**c**) State 3, state 4, FCCP-induced and GDP-sensitive OCR in mitochondria isolated from BAT of WT mice 16 h after bortezomib (2.5 mg/kg) or DMSO at 22 °C (Biol. replicates n=4 for state 3 and state 4 and n=3 for FCCP and GDP, **P*<0.05 by T-Test). (**d-f**) OCR in brown adipocytes 16 h after epoxomicin (100 nM) or DMSO treatment (representative traces in (d), tech. replicates n=4 in (e,f), **P*<0.05 by T-Test). (**g**) Nrf1 protein levels in BAT after 6 h carfilzomib (4 mg/kg) or DMSO treatment (22 °C, lanes represent biological replicates, cropped images). (**h**) Nrf1 protein levels in control brown adipocytes or cells overexpressing Nrf1. Cells were treated with 250 nM epoxomicin or DMSO for 6 h (biol. Replicates n=3, cropped images). (**i**) Tissue mRNA levels of *Nfe2l1* in WT mice after adaptation to 30 °C or 4 °C for 7 days (Biol. replicates n=4, **P*<0.05 by T-Test with Holm-Sidak correction for multiple testing, SkeMus: Skeletal muscle).

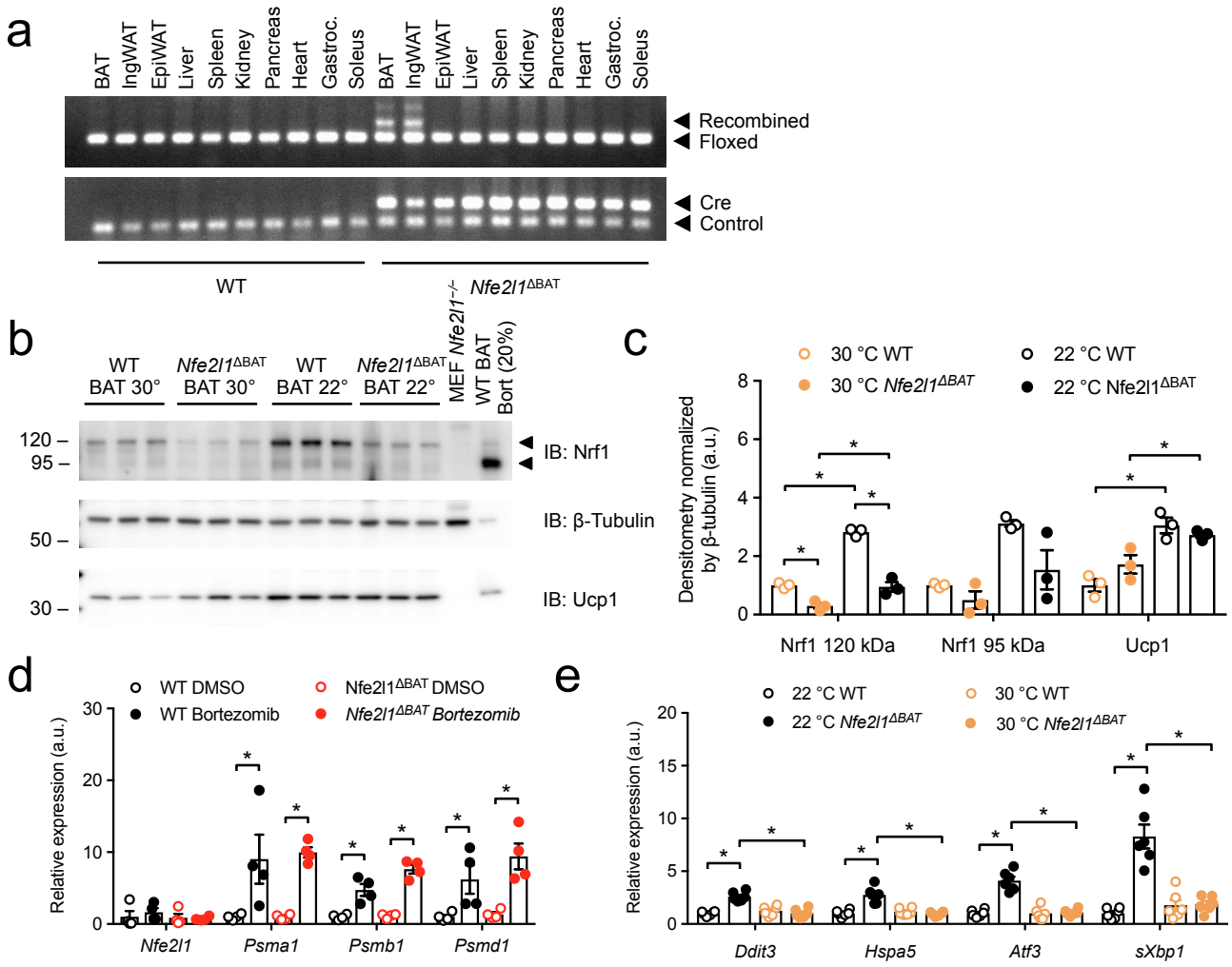

Supplementary Fig. 3 Validation of the *Nfe2l1*$^{\Delta BAT}$ model. (**a**) PCR detection of cre recombinase-mediated recombination of the floxed *Nfe2l1* locus (upper panel) as well as cre genotyping (lower panel) in selected tissues (cropped images). (**b,c**) Nrf1 and Ucp1 protein levels determined by immunoblot analysis (cropped images) in BAT (**b**) and quantified (**c**) from WT and *Nfe2l1*$^{\Delta BAT}$ mice born and raised at 30 °C or 22 °C (n=3 biol. replicates). Lysates from Nrf1-deficient mouse embryonic fibroblasts (MEFs) or BAT from bortezomib-treated mice (20 % protein amount loaded on the gel) served as controls. (**d**) mRNA levels of proteasome subunits in the livers of WT or *Nfe2l1*$^{\Delta BAT}$ mice after 16 h bortezomib (2.5 mg/kg) or DMSO treatment (22 °C; biol. replicates n=4, normalized to ΔCT, **P*<0.05 by 2-way ANOVA). **(e)** mRNA levels of stress markers in BAT of WT or *Nfe2l1*$^{\Delta BAT}$ mice born at 22 °C and then placed at 30 °C for 7 days (Biol. replicates n=6, normalized to *18s*, **P*<0.05 by 2-way ANOVA).

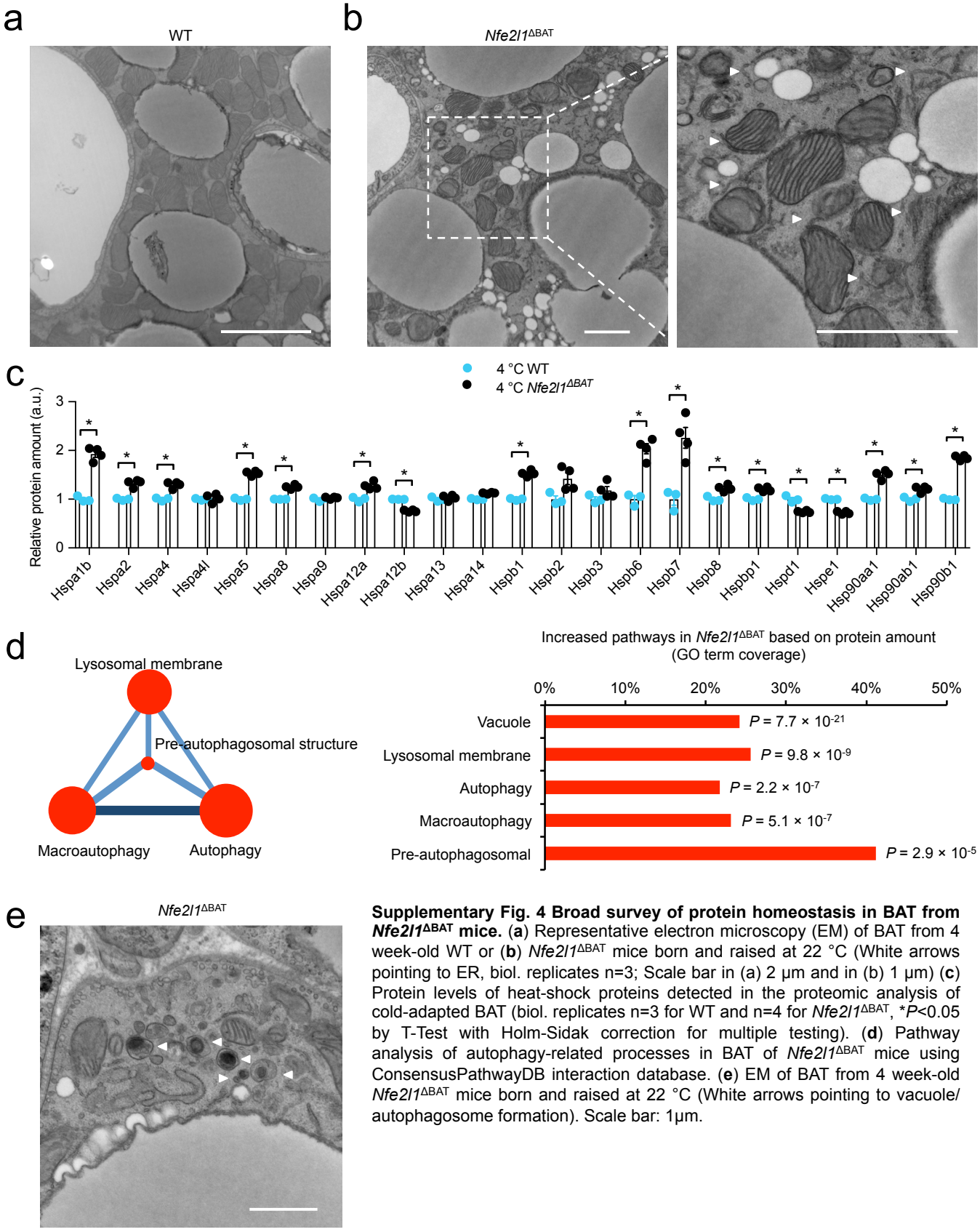

Supplementary Fig. 4 Broad survey of protein homeostasis in BAT from *Nfe2l1*$^{\Delta BAT}$ mice. (**a**) Representative electron microscopy (EM) of BAT from 4 week-old WT or (**b**) *Nfe2l1*$^{\Delta BAT}$ mice born and raised at 22 °C (White arrows pointing to ER, biol. replicates n=3; Scale bar in (a) 2 µm and in (b) 1 µm) (**c**) Protein levels of heat-shock proteins detected in the proteomic analysis of cold-adapted BAT (biol. replicates n=3 for WT and n=4 for *Nfe2l1*$^{\Delta BAT}$, *P<0.05 by T-Test with Holm-Sidak correction for multiple testing). (**d**) Pathway analysis of autophagy-related processes in BAT of *Nfe2l1*$^{\Delta BAT}$ mice using ConsensusPathwayDB interaction database. (**e**) EM of BAT from 4 week-old *Nfe2l1*$^{\Delta BAT}$ mice born and raised at 22 °C (White arrows pointing to vacuole/ autophagosome formation). Scale bar: 1µm.

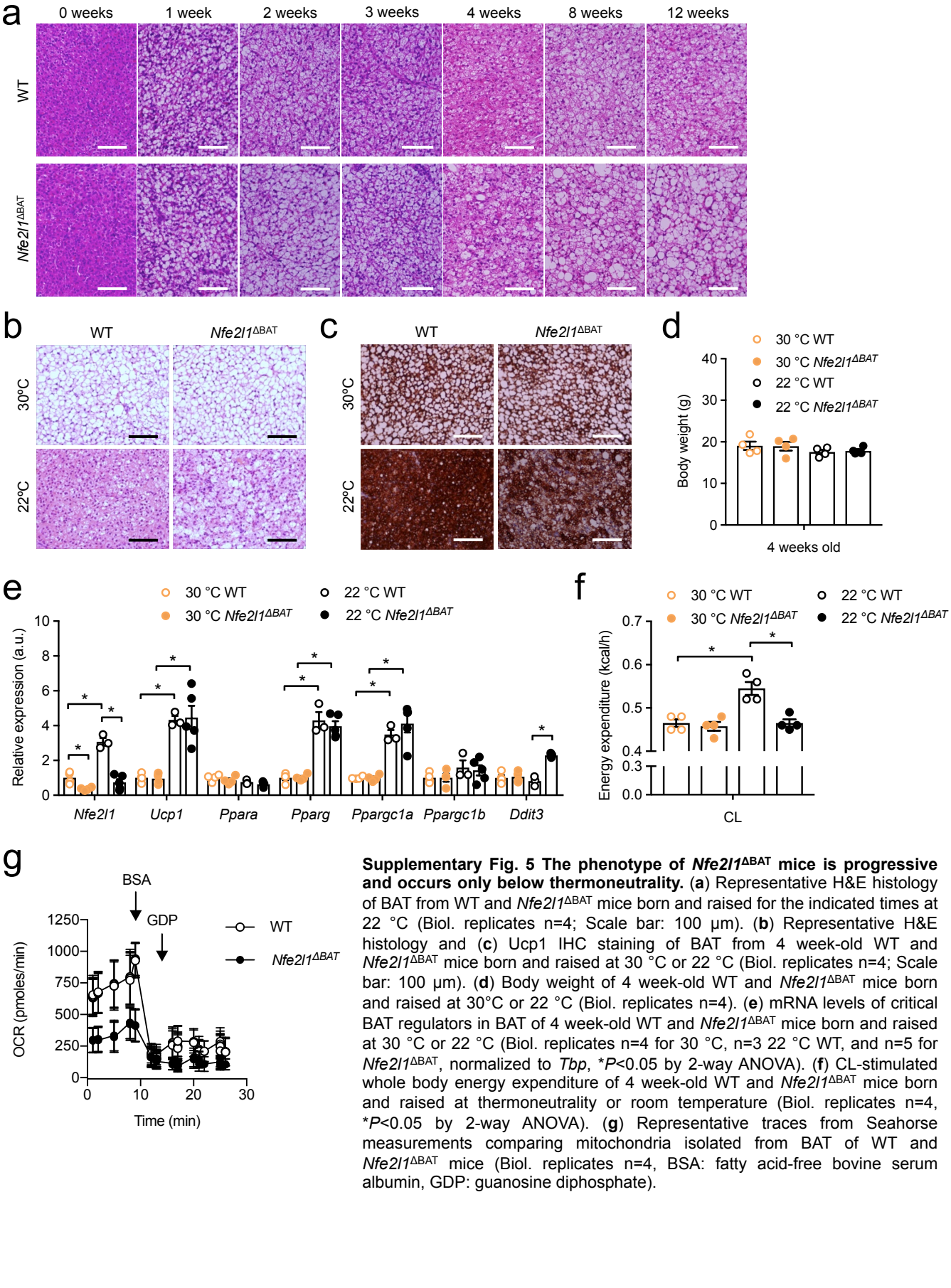

Supplementary Fig. 5 The phenotype of *Nfe2l1*$^{\Delta BAT}$ mice is progressive and occurs only below thermoneutrality. (**a**) Representative H&E histology of BAT from WT and *Nfe2l1*$^{\Delta BAT}$ mice born and raised for the indicated times at 22 °C (Biol. replicates n=4; Scale bar: 100 µm). (**b**) Representative H&E histology and (**c**) Ucp1 IHC staining of BAT from 4 week-old WT and *Nfe2l1*$^{\Delta BAT}$ mice born and raised at 30 °C or 22 °C (Biol. replicates n=4; Scale bar: 100 µm). (**d**) Body weight of 4 week-old WT and *Nfe2l1*$^{\Delta BAT}$ mice born and raised at 30°C or 22 °C (Biol. replicates n=4). (**e**) mRNA levels of critical BAT regulators in BAT of 4 week-old WT and *Nfe2l1*$^{\Delta BAT}$ mice born and raised at 30 °C or 22 °C (Biol. replicates n=4 for 30 °C, n=3 22 °C WT, and n=5 for *Nfe2l1*$^{\Delta BAT}$, normalized to *Tbp*, **P*<0.05 by 2-way ANOVA). (**f**) CL-stimulated whole body energy expenditure of 4 week-old WT and *Nfe2l1*$^{\Delta BAT}$ mice born and raised at thermoneutrality or room temperature (Biol. replicates n=4, **P*<0.05 by 2-way ANOVA). (**g**) Representative traces from Seahorse measurements comparing mitochondria isolated from BAT of WT and *Nfe2l1*$^{\Delta BAT}$ mice (Biol. replicates n=4, BSA: fatty acid-free bovine serum albumin, GDP: guanosine diphosphate).

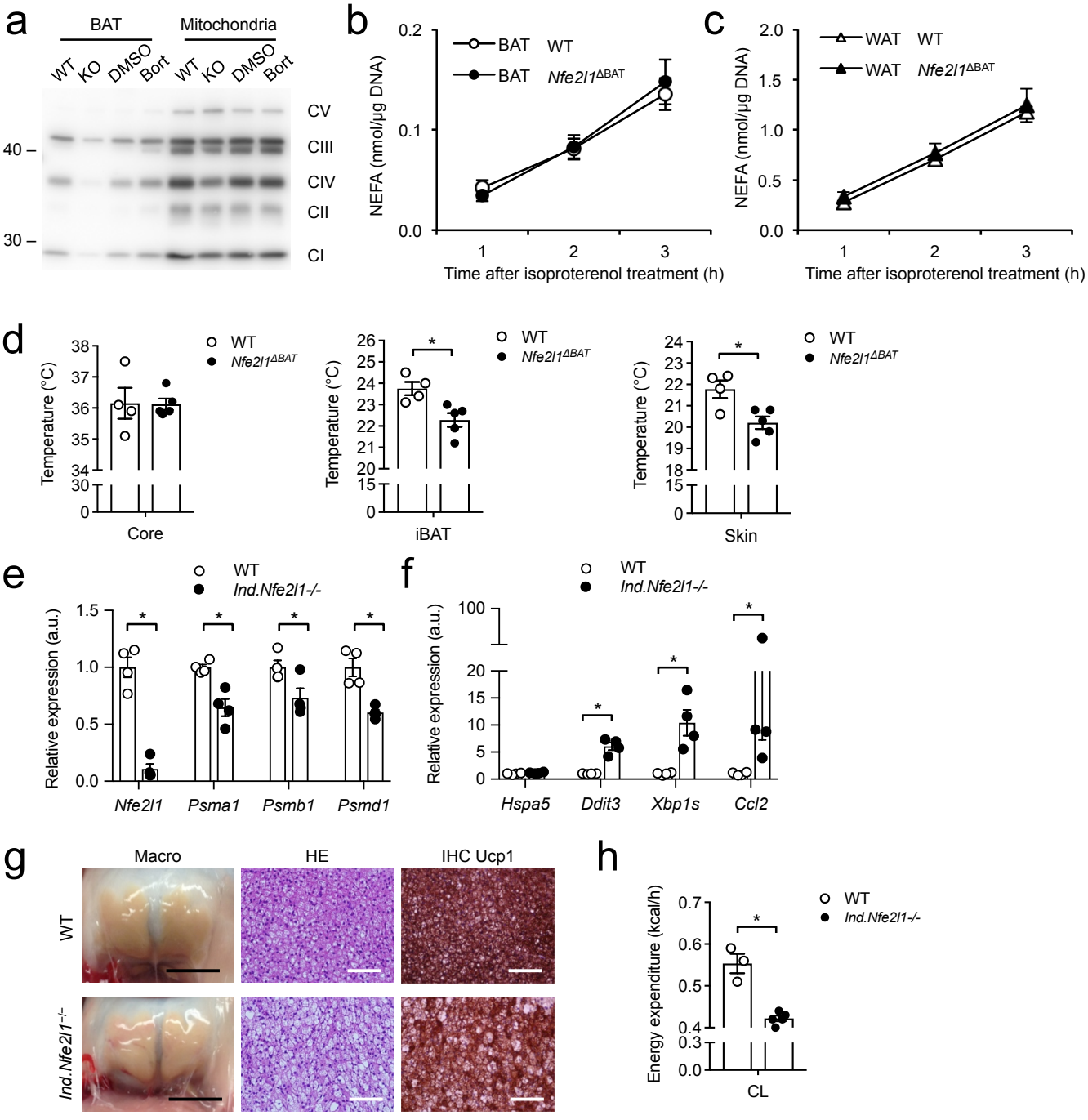

Supplementary Fig. 6 Inducible Nrf1 deletion results in stress pathway activation and BAT dysfunction. (**a**) Immunoblot analysis of OXPHOS complexes (CI-V) in BAT or isolated mitochondrial from WT and *Nfe2l1*$^{\Delta BAT}$ mice (KO) as well as DMSO or bortezomib (bort)-treated animals, respectively (cropped images). (**b,c**) *Ex vivo* lipolysis assay measuring isoproterenol-stimulated non-esterified fatty acid (NEFA) release from (b) BAT and (c) WAT explants from 6 week-old WT and *Nfe2l1*$^{\Delta BAT}$ mice born at 22 °C (Biol. replicates n=3). (**d**) Measurement of body core, BAT and skin temperature in WT and *Nfe2l1*$^{\Delta BAT}$ mice adapted to cold for 7 days. (biol. replicates, WT n=4, *Nfe2l1*$^{\Delta BAT}$ n=5, **P*<0.05 by T-Test). (**e,f**) BAT mRNA levels in WT and mice, 7 days after the *Nfe2l1* gene was disrupted in adult mice conditionally by tamoxifen (*Ind.Nfe2l1*$^{-/-}$) at room temperature (biol. replicates n=4, normalized to *Rn18s*, **P*<0.05 by (e) T-Test or (f) Mann-Whitney U-Test). (**g**) Representative photographs (Scale bar: 5 mm), H&E histology and Ucp1 IHC (Scale bar: 100 µm) of iBAT from WT and *Ind.Nfe2l1*$^{-/-}$ mice (**h**) CL-stimulated whole body energy expenditure in WT and *Ind.Nfe2l1*$^{-/-}$ (biol. replicates n=3 for WT and n=5 for *Ind.Nfe2l1*$^{-/-}$ mice, **P*<0.05 by T-Test).

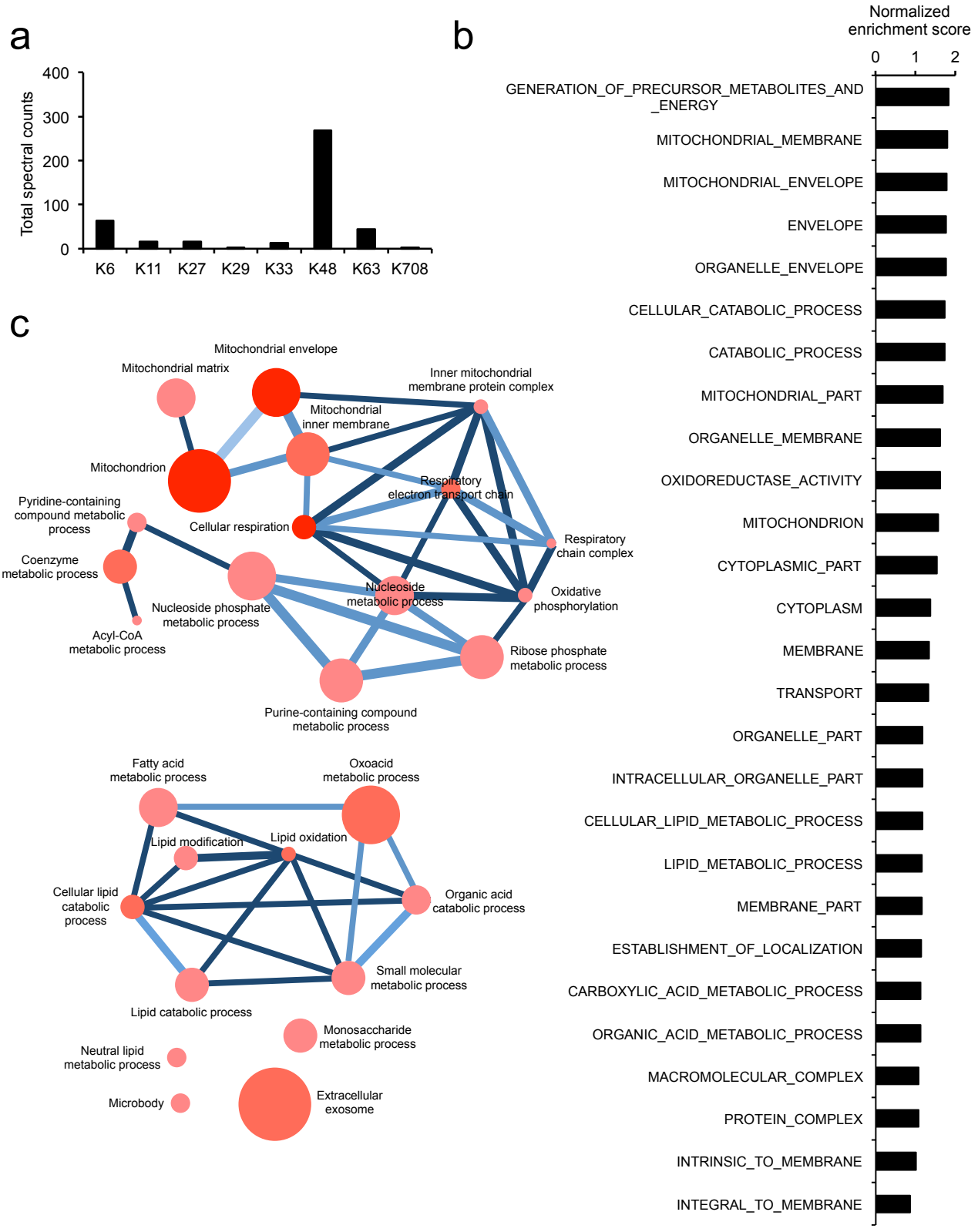

Supplementary Fig. 7 Analysis of the BAT ubiquitome. (**a**) Proteomic quantification of ubiquitin modifications. (**b**) Gene set enrichment analysis (GSEA) of hyperubiquitinated proteins in BAT of *Nfe2l1*$^{\Delta BAT}$ mice (**c**) Pathway analysis of hyperubiquitinated proteins in BAT of *Nfe2l1*$^{\Delta BAT}$ mice using ConsensusPathwayDB interaction database.

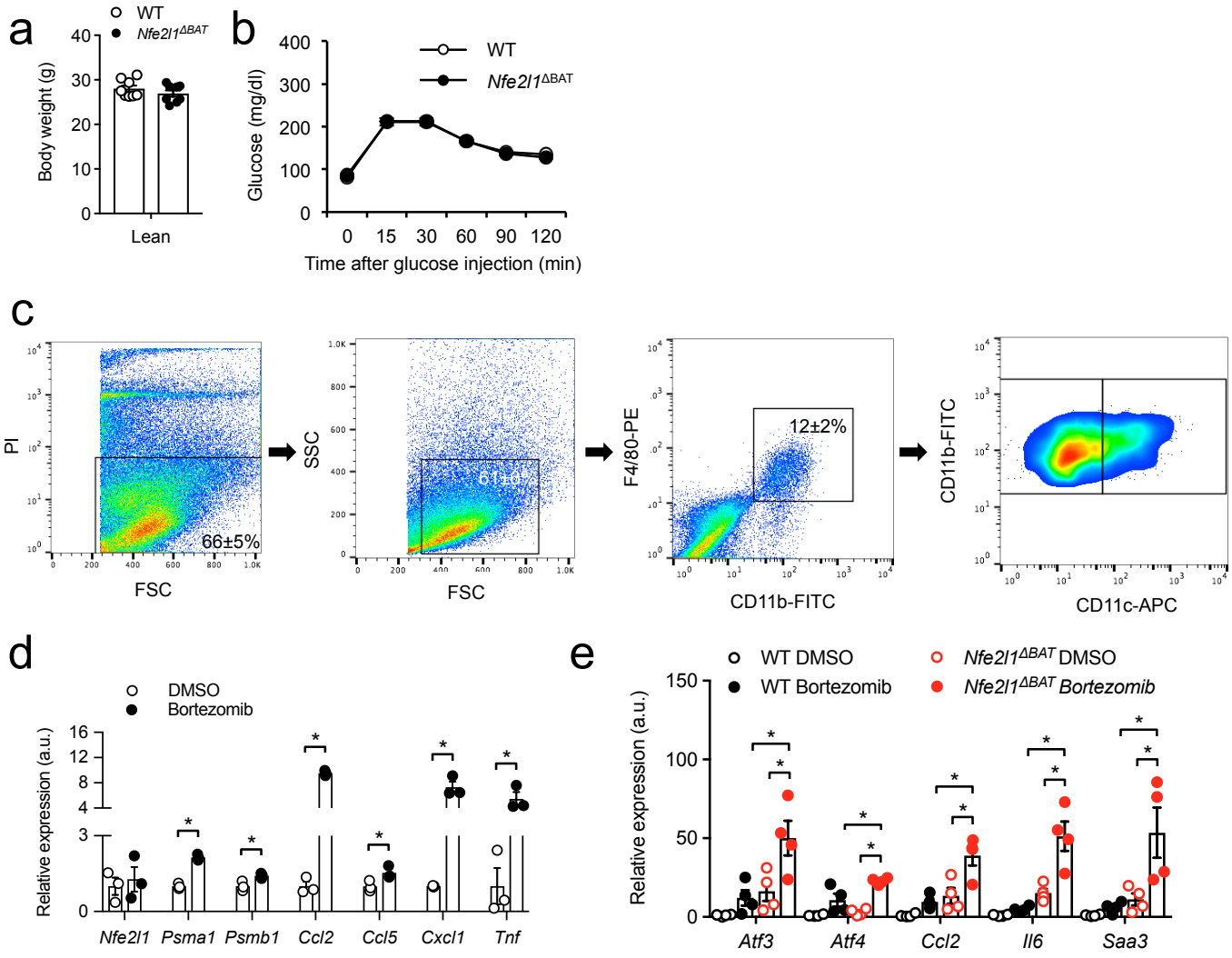

Supplementary Fig. 8 Metabolic phenotype of lean *Nfe2l1*$^{\Delta BAT}$ mice. (**a**,**b**) Body weight (**a**) and glucose tolerance (**b**, 1 g/kg) in lean WT and *Nfe2l1*$^{\Delta BAT}$ mice born and raised at room temperature (Biol. replicates n=8). (**c**) Representative gating strategy for macrophage flow cytometry analysis in BAT. (**d**) Gene expression analysis of cultured brown adipocytes after 8h treatment with DMSO or 20 nM bortezomib. (Biol. replicates n=3, normalized to *Tbp*, **P*<0.05 by T-Test). (**e**) mRNA levels of inflammatory markers in iBAT of WT or *Nfe2l1*$^{\Delta BAT}$ mice after 16 h bortezomib (2.5 mg/kg) or DMSO control treatment (22 °C; biol. replicates n=4, normalized to *Rn18s*, **P*<0.05 by 2-way ANOVA).

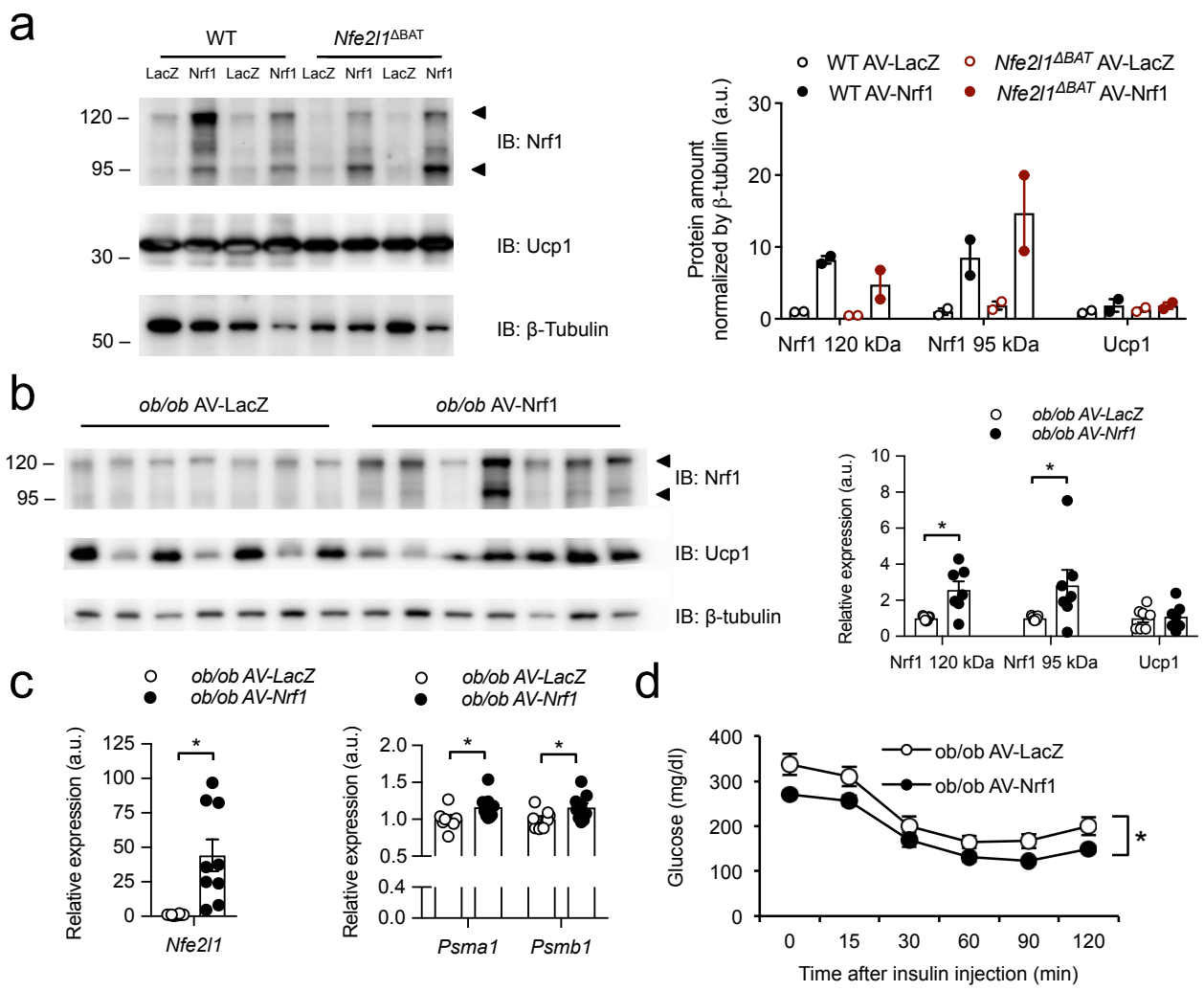

Supplementary Fig. 9 Adenoviral manipulation of BAT. (**a**) Nrf1 and Ucp1 protein levels determined by immunoblot analysis in BAT of WT and *Nfe2l1*$^{\Delta BAT}$ mice contralateral BAT-injected with AV-LacZ or AV-Nrf1 (Biol. replicates n=2, same interscapular BAT depot is shown for one mouse, cropped images). (**b**) Nrf1 and Ucp1 protein levels determined by immunoblot analysis in BAT of *ob/ob* mice BAT-injected with either AV-LacZ or AV-Nrf1 (Biol. replicates n=7, **P*<0.05 by Mann-Whitney U-Test, cropped images). (**c**) mRNA levels of *Nfe2l1* and proteasome subunits in BAT of *ob/ob* mice BAT-injected with either AV-LacZ or AV-Nrf1 (Biol. replicates AV-LacZ n=8, AV-Nrf1 n=9, normalized to *Tbp*, **P*<0.05 by T-Test). (**d**) Insulin tolerance test in *ob/ob* mice BAT-injected with AV-LacZ or AV-Nrf1 (Biol. replicates AV-LacZ n=8, AV-Nrf1 n=9, **P*<0.05 by T-Test on AUC).

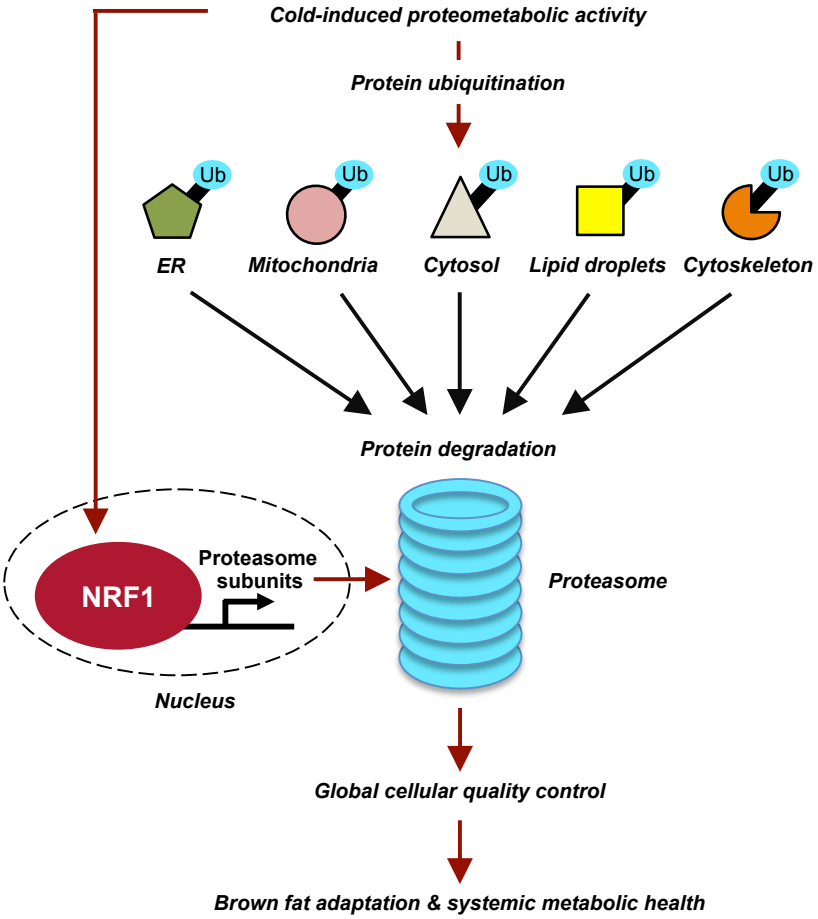

Supplementary Fig. 10 Schematic model summarizing the main findings of this study. Cold adaptation introduces an unusual and extreme metabolic burden on brown fat cells. The mechanism by which brown fat cells adapt to increased turnover of proteins, metabolites as well as synthesis and breakdown of cellular components is unknown. Here we show that proteasomal degradation of ubiquitinated proteins is a fundamental adaptive mechanism by which cellular integrity and quality control is achieved and identify the cold-inducible transcription factor NRF1 as the critical driver of proteasomal activity, brown fat metabolic adaptation and systemic homeostasis. Nrf1 loss and gain-of-function in preclincal models of obesity-induced insulin resistance demonstrate that Nrf1 is a guardian of metabolic health and a promising future drug target.

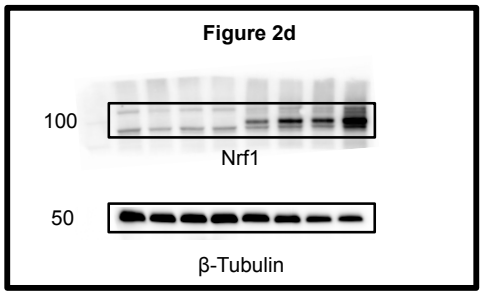

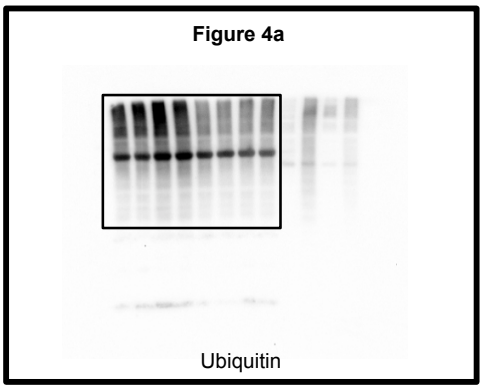

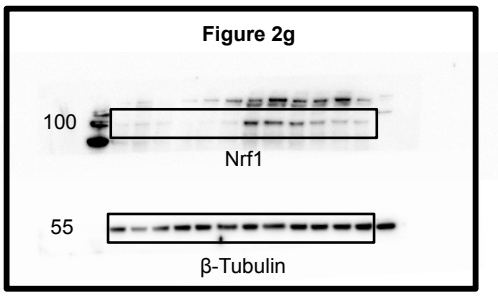

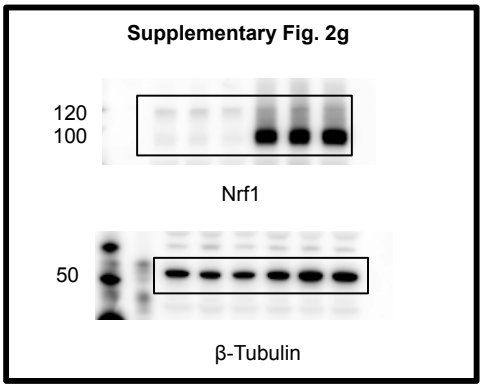

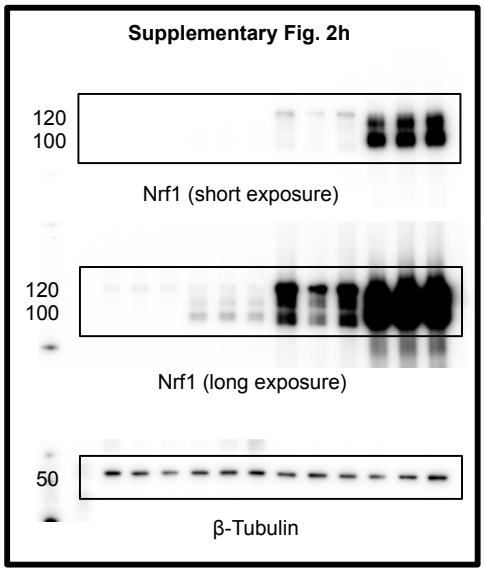

Supplementary Fig. 11 Uncropped immunoblot pictures #1.

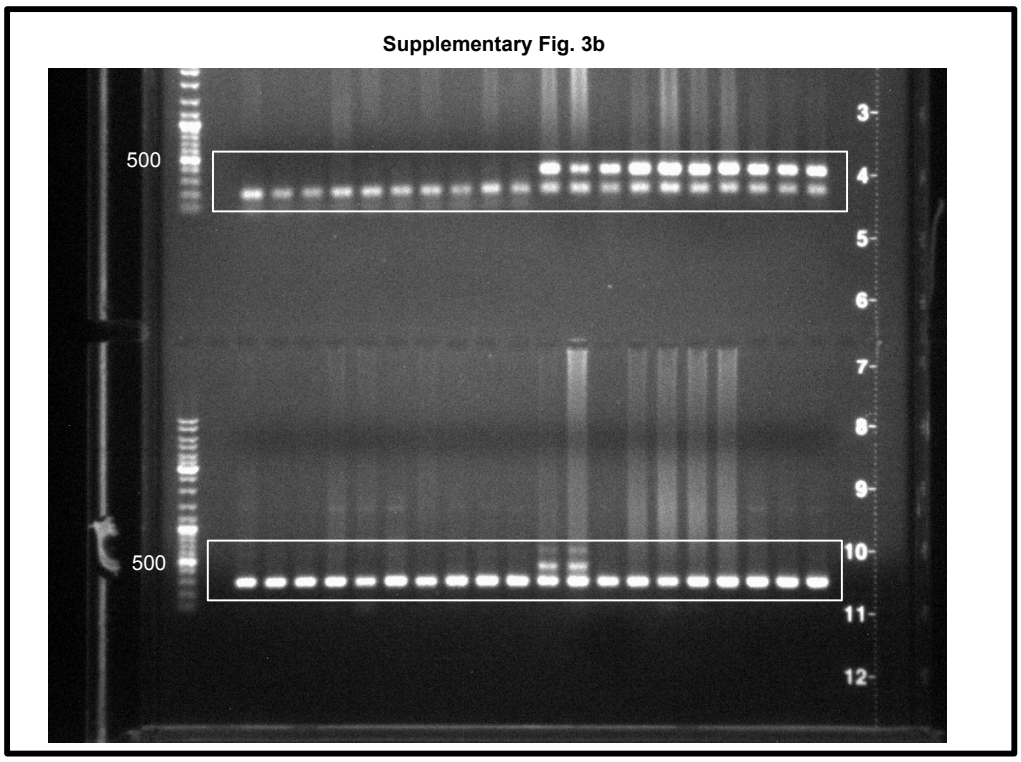

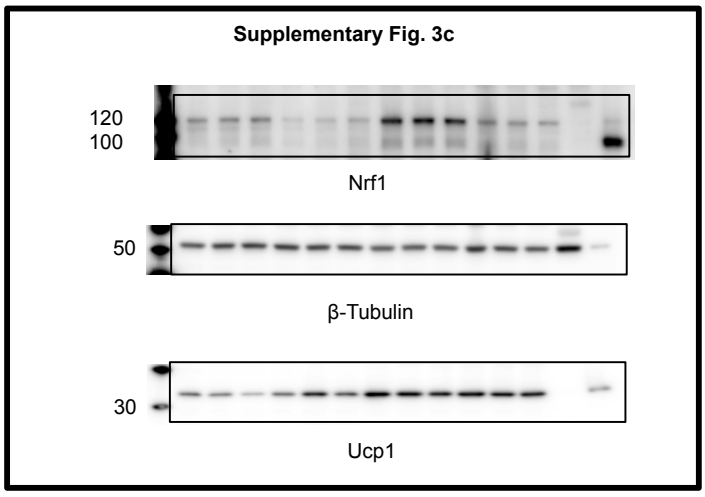

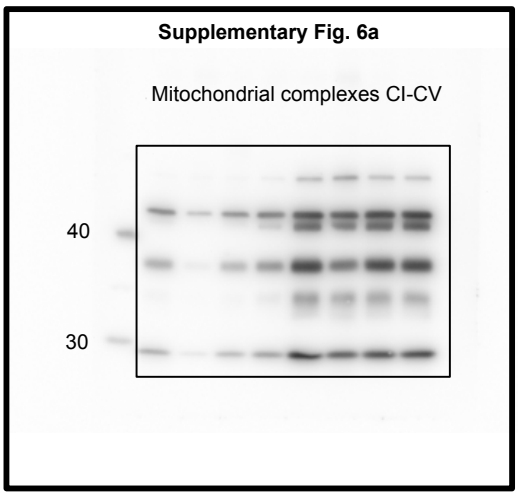

Supplementary Fig. 12 Uncropped gel and immunoblot pictures #2.

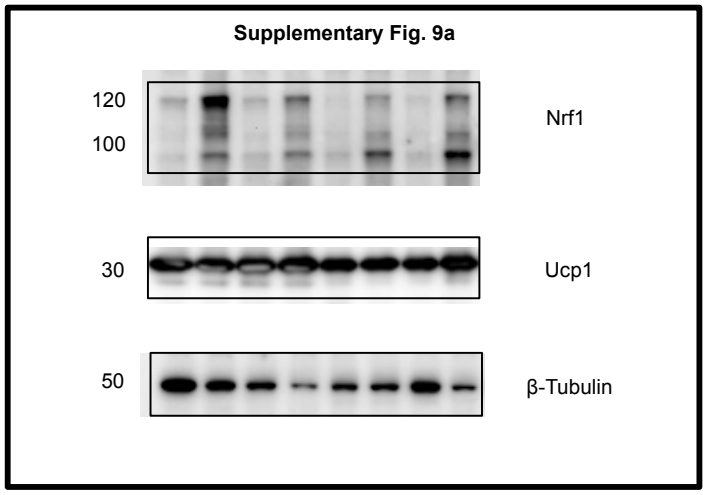

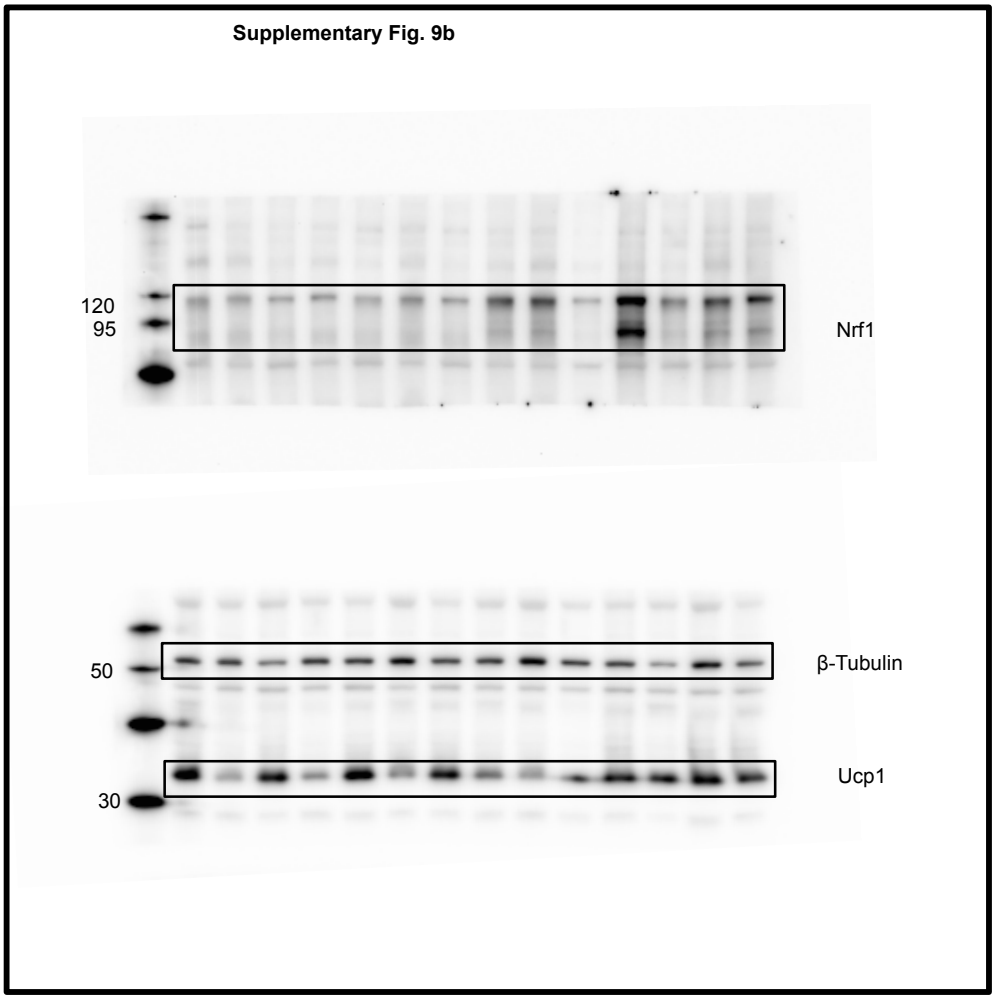

Supplementary Fig. 13 Uncropped immunoblot pictures #3.

Supplementary Methods

Immunohistochemistry. We performed immunohistochemistry on paraffin slides. We mounted sections on adhesion slides, deparaffinized and rehydrated using a standard protocol (2 x Xylene, 2 x 100 % Ethanol, 95 % v/v Ethanol, 70 % v/v Ethanol, 50 % v/v ethanol, water, 5 min each). To block endogenous peroxidase activity, we incubated sections in 3 % v/v H_2O_2 in PBS for 10 min. We performed antigen retrieval by boiling the slides in Citrate buffer (10 mM sodium citrate, 0.05 % v/v Tween 20, pH 6) in a microwave oven for 10 min. We cooled slides down to room temperature for 20 min, rinsed these with PBS and then placed them in a humidity chamber for blocking and permeabilization in blocking buffer (2 % v/v goat serum, 1 % w/v BSA, 0.1 % v/v Triton X-100, 0.05 % v/v Tween 20 in PBS) for 1.5 h at room temperature. We incubated the slides with the primary antibody (anti-UCP1, abcam # 10981), diluted in 1 % w/v BSA, 0.05 % v/v sodium azide in PBS over night at 4 °C. After the primary antibody incubation, we washed the slides with PBS for 3 x 10 min and then incubated them with goat anti-rabbit horseradish peroxidase secondary antibody (Santa Cruz #2030) at a 1:500 dilution for 1 h at room temperature. After the secondary antibody incubation, sections were washed with PBS for 3 x 10 min. We performed staining using a 3,3'-diaminobenzidine (DAB) substrate kit (abcam) following the manufacturer's instructions. After DAB staining, we rinsed the slides with PBS to stop the chromogenic reaction and counterstained with hematoxylin QS (Vector Laboratories) for 2 min. We incubated the slides under running tap water for 10 min, after which the slides were dehydrated in 50 % v/v Ethanol, 70 % v/v Ethanol, 95 % v/v Ethanol, 2 x 100 % Ethanol and 2 x Xylene for 5 min each. Mounting was performed using Permount (Electron Microscopy Sciences).

Macrophage isolation and flow cytometry. We performed the isolation of stromal vascular fraction (SVF) of BAT containing the immune cells as previously described[71] with some modifications in 1 representative cohort of HFD-fed mice. Briefly, we minced

the interscapular BAT depot from individual mice and incubated the tissue in DMEM containing collagenase I and II (Calbiochem, 2 mg/ml each) for 40 min at 37 °C with 120 rpm shaking. We stopped the reaction with FACS buffer (PBS containing 5% FBS) and filtered the suspensions through 100 μm cell strainers (BD Falcon). The cell suspensions were centrifuged at 2500 rpm for 5 min. We re-suspended the pellet in FACS buffer and filtered it through a 40 μm cell strainer (BD Falcon). We centrifuged the cell suspension at 3500 rpm for 5 min and the pellet was incubated for 5 min in erythrocyte-lysing buffer (Sigma). Finally, we suspended the cells in FACS buffer. The antibodies (1:100) used for the analysis of the SVF of BAT were anti-CD11b (eBioscience M1/70), anti-F4/80 (Biolegend BM8), anti-CD11c (Biolegend N418). A representative gating strategy can be found in Supplementary Fig. 7d. We analyzed the data using FACS Calibur (BD Falcon) and FlowJo software (FlowJo). We expressed the total number of macrophages per interscapular BAT depot per mouse and the M1/2 polarization within these fractions was expressed as the percentage of total macrophages.

Sample preparation and liquid chromatography-MS3 spectrometry for proteomics. BAT samples from 1 representative cohort of mice for multiplexed quantitative mass spectrometry analysis were processed and analyzed through the Thermo Fisher Scientific Center for Multiplexed Proteomics at Harvard Medical School. Immunoprecipitation of diGly-containing peptides was performed as described previously[72]. Samples for proteomic analysis were prepared as previously described[73] with the following modification. All solutions are reported as final concentrations. Lysis buffer (8 M Urea, 1 % SDS, 50 mM Tris pH 8.5, Protease and Phosphatase inhibitors from Roche) was added to the tissue to achieve a cell lysate with a protein concentration between 2-8 mg/mL. In order to facilitate tissue lysis a mechanical tissue grinder was used to homogenize the tissue. A micro-BCA assay (Pierce) was used to determine the final protein concentration in the cell lysate. Proteins were reduced and alkylated as previously

described. Proteins were precipitated using methanol-chloroform. In brief, 4 volumes of methanol were added to the cell lysate, followed by 1 volume of chloroform, and finally 3 volumes of water. The mixture was vortexed and centrifuged to separate the chloroform phase from the aqueous phase. The precipitated protein was washed with one volume of ice-cold methanol. The washed precipitated protein was allowed to air dry. Precipitated protein was resuspended in 4 M Urea, 50 mM Tris pH 8.5. Proteins were first digested with LysC (1:50; enzyme:protein) for 12 h at 25 °C. The LysC digestion was diluted down to 1 M Urea, 50 mM Tris pH8.5 and then digested with trypsin (1:100; enzyme:protein) for another 8 h at 25 °C. Peptides were desalted using a C_{18} solid phase extraction cartridges as previously described. Dried peptides were resuspended in 200 mM EPPS, pH 8.0. Peptide quantification was performed using the micro-BCA assay (Pierce). The same amount of peptide from each condition was labeled with tandem mass tag (TMT) reagent (1:4; peptide:TMT label) (Pierce). The 10-plex labeling reactions were performed for 2 h at 25 °C. Modification of tyrosine residue with TMT was reversed by the addition of 5 % hydroxyl amine for 15 min at 25 °C. The reaction was quenched with 0.5 % TFA and samples were combined at a 1:1:1:1:1:1:1:1:1:1 ratio. Combined samples were desalted and offline fractionated into 24 fractions as previously described. 12 of the 24 peptide fraction from the basic reverse phase step (every other fraction) were analyzed with an LC-MS3 data collection strategy[74] on an Orbitrap Fusion mass spectrometer (Thermo Fisher Scientific) equipped with a Proxeon Easy nLC 1000 for online sample handling and peptide separations. Approximately 5 µg of peptide resuspended in 5 % formic acid + 5 % acetonitrile was loaded onto a 100 µm inner diameter fused-silica micro capillary with a needle tip pulled to an internal diameter less than 5 µm. The column was packed in-house to a length of 35 cm with a C_{18} reverse phase resin (GP118 resin 1.8 µm, 120 Å, Sepax Technologies). The peptides were separated using a 180 min linear gradient from 3 % to 25 % buffer B (100 % ACN + 0.125 % formic acid) equilibrated with buffer A (3 % ACN + 0.125 % formic acid) at a flow rate of

400 nL/min across the column. The scan sequence for the Fusion Orbitrap began with an MS1 spectrum (Orbitrap analysis, resolution 120,000, 400−1400 *m/z* scan range with quadrapole isolation, AGC target 2×10^5, maximum injection time 100 ms, dynamic exclusion of 90 seconds). 'Top N" (the top 10 precursors) was selected for MS2 analysis, which consisted of CID ion trap analysis, AGC 8×10^3, NCE 35, maximum injection time 150 ms), and quadrapole isolation of 0.5 Da for the MS1 scan. The top ten fragment ion precursors from each MS2 scan were selected for MS3 analysis (synchronous precursor selection), in which precursors were fragmented by HCD prior to Orbitrap analysis (NCE 55, max AGC 1×10^5, maximum injection time 150 ms, MS2 quadrapole isolation was set to 2.5 Da, resolution 60,000. For diGly-enriched fractions the scan sequence for the Fusion Orbitrap began with an MS1 spectrum (Orbitrap analysis, resolution 120,000, 400−1250 *m/z* scan range with quadrapole isolation, AGC target 5×10^5, maximum injection time 100 ms, dynamic exclusion of 60 seconds). 'Top N" (the top 10 precursors) was selected for MS2 analysis, which consisted of Orbitrap analysis with quadrapole isolation of 0.5 Da for precursor selection, 1.5×10^4 resolution, AGC 1.5×10^5, NCE 35, maximum injection time 300 ms), and for the MS1 scan. The top three fragment ion precursors from each MS2 scan were selected for MS3 analysis (synchronous precursor selection), in which precursors were fragmented by HCD prior to Orbitrap analysis (NCE 55, max AGC 1×10^5, maximum injection time 500 ms, MS2 quadrapole isolation was set to 2.5 Da, resolution 60,000. MS/MS data were searched against a Uniprot mouse database (August 2013) with both the forward and reverse sequences using the SEQUEST algorithm. Further data processing steps included controlling peptide and protein level false discovery rates, assembling proteins from peptides, and protein quantification from peptides. Statistical significance for proteins and ubiquitin sites was calculated using the Benjamini-Hochberg method for multiple hypothesis correction. For the differential BAT ubiquitome we divided the relative intensities for ubiquitin-modified proteome by the relative intensities of the conventional

proteome. Several proteins, for which we found ubiquitination sites from the ubiquitin-modified proteome were not found in the conventional proteome and therefore were excluded from the differential ubiquitome analysis. We performed pathway analysis using Gene Set Enrichment Analysis (GSEA, www.broadinstitute.org/gsea) with default settings[75,76]. To increase signal-to-noise ratio we included only sites that were at least significantly 2-fold higher in *Nfe2l1*$^{\Delta BAT}$ BAT compared to WT and if multiple sites were found per individual protein only the site displaying the highest ubiquitination relative to the WT was included. For visualization of the pathway analysis we used the ConsensusPathDB interaction database (CPDB; http://cpdb.molgen.mpg.de/MCPDB) and included the proteins listed in the GSEA analysis with a significance cut-off of 6.92×10^{-15} and a relative overlap of 0.4 for GO term level 4.

SWIR quantum dots and SWIR in vivo imaging. For the synthesis of SWIR-emitting quantum dots (QDs), 4 mmoles of indium(III) acetate and 16 mmoles of oleic acid were mixed in 20 mL 1-octadecene (ODE) and degassed at RT for 30 minutes. The mixture was heated to 115 °C under vacuum for another 60 minutes and then heated to 295 °C under nitrogen. In a glovebox 0.2 mmoles $(TMGe)_3As$[77,78] were dissolved in 4 ml trioctylphosphine (TOP) and subsequently injected into the solution. After 10 min a 0.17 M solution of $(TMGe)_3As$ in ODE was injected for 11 minutes at a speed of 8 mL per h. The heat was removed and the growth solution was transferred to a glovebox and purified by 2 precipitation/redispersion cycles. Purified InAs QDs (71 nmoles) in hexanes were transferred to a mixture of 2 mL ODE and 2 mL oleylamine. The solution was degassed for 30 min at RT and another 10 min at 110 °C. Subsequently, the solution was heated to 280 °C for the shell growth. As soon as the mixture reached 240 °C, shell precursor injection was started. 1 mL of a 0.05 M cadmium(II) oleate 0.3 M oleic acid solution in ODE, and 1 mL of a 0.05 M solution of TOP-Se in TOP/ODE (1:19) were injected over 40 minutes. InAsCdSe core-shell QDs were purified using the above

described procedure and the resulting QDs (ca. 60 nmoles) were redispersed in 2 mL ODE and 2 mL Oleylamine. To that solution 1.2 mL of a 0.05 M cadmium(II) oleate 0.3 M oleic acid solution in ODE and 1.2 mL of a 0.045 M sulfur solution in ODE were added within 48 min. InAsCdSeCdS core-shell-shell QDs were purified using the procedure described above and exhibited a fluorescence peak at 1129 nm and a fluorescence quantum yield of 37 %. QD-labelled recombinant triglyceride-rich lipoproteins were generated by a previously reported procedure[79]. Briefly, for incorporating the QDs into the recombinant lipoproteins, 20 mg of lipid extract (approximately 80 % triglycerides, 10 % cholesterol and 10 % phospholipids) were dissolved in chloroform and mixed with 1 mg (dry weight) InAsCdSeCdS core-shell-shell QDs. The solvent was removed and the lipoproteins were formed in 2 mL PBS or isotonic saline by sonication with a probe sonicator for 10 minutes. Potential aggregates were removed by filtration using a 0.45 μm filter prior to injection. For the SWIR imaging set-up, we coupled a 10 W 808 nm laser (Opto Engine; MLL-N-808) in a 910 μm-core metal-cladded multimode fiber (Thorlabs; MHP910L02). The output from the fiber is passed through a ground-glass plate (Thorlabs; DG20-220-MD) to provide uniform illumination over the working area. We used a 4 in square first-surface silver mirror (Edmund Optics; Part No 84448) to direct the emitted light through two colored glass 1000 nm long-pass filters (Thorlabs) to a Princeton Instruments Nirvana equipped with a C-mount camera lenses (Navitar). The whole assembly was surrounded by a partial enclosure to eliminate excess light while enabling manipulation of the field of view during operation. Cold exposure (4 °C) was performed in single cages for 24 h including a 4 h fasting period. For in vivo imaging to measure metabolic rates mice were anesthetized (150 mg/kg ketamine and 15 mg/kg xylazine) mice, their fur removed (Nair) and placed into the SWIR imaging setting. QD-labeled lipoproteins were injected via a tail vein catheter with a syringe pump at a rate of 13.3 μL/mL (2 mg lipid per mouse) and SWIR signal was recorded over time as well as after the injection from dissected iBAT.

Transmisson electron microscopy. 4-week-old mice from 3 independent cohorts were anesthetized (300 mg/kg ketamine and 30 mg/kg xylazine) and transcardially perfused first with 0.9 % w/v NaCl and then with electron microscopy grade fixative buffer containing: 2.5 % w/v glutaraldehyde, 2.5 % w/v paraformaldehyde in 0.1 M sodium cacodylate buffer, pH 7.4 (Electron Microscopy Science). 2 min after perfusion, small pieces (1 to 2 mm cubes) of tissue were stored in the same fixative buffer described above until further processing. The tissues were then washed in 0.1 M cacodylate buffer and postfixed with 1 % w/v osmiumtetroxide (OsO4)/1.5 % w/v potassium ferrocyanide (K2FeCN6) for 3 h, washed in water three times and incubated in 1 % w/v uranyl acetate in maleate buffer (pH 5.2) for 1 h followed by 3 washes in maleate buffer and subsequent dehydration in grades of ethanol (10 min each; 50 %, 70 %, 90 %, 2 × 10 min 100 %), followed by 3 propylene oxide washes over one hour. Then the samples were placed in 50 % w/w propylene oxide with plastic mixture including catalyst overnight. The following day, samples were embedded in TAAB 812 Resin mixture (Marivac Ltd., Nova Scotia, Canada) and polymerized at 60 °C for 48 h. Ultrathin sections (80 nm) were generated using a Leica Ultracut microtome, picked up on 100 μm mesh formvar/carbon copper grids, stained with 0.2 % w/v lead citrate and examined in a TecnaiG2 Spirit BioTWIN microscope. Images were recorded with an AMT 2k CCD camera.

References:

70. Nguyen, K. D. *et al.* Alternatively activated macrophages produce catecholamines to sustain adaptive thermogenesis. *Nature* **480**, 104-108, doi:10.1038/nature10653 (2011).
71. Rose, C. M. *et al.* Highly Multiplexed Quantitative Mass Spectrometry Analysis of Ubiquitylomes. *Cell Syst* **3**, 395-403 e394, doi:10.1016/j.cels.2016.08.009 (2016).
72. Weekes, M. P. *et al.* Quantitative temporal viromics: an approach to investigate host-pathogen interaction. *Cell* **157**, 1460-1472, doi:10.1016/j.cell.2014.04.028 (2014).
73. McAlister, G. C. *et al.* MultiNotch MS3 enables accurate, sensitive, and multiplexed detection of differential expression across cancer cell line proteomes. *Anal Chem* **86**, 7150-7158, doi:10.1021/ac502040v (2014).

74. Mootha, V. K. *et al.* PGC-1alpha-responsive genes involved in oxidative phosphorylation are coordinately downregulated in human diabetes. *Nat Genet* **34**, 267-273, doi:10.1038/ng1180 (2003).

75. Subramanian, A. *et al.* Gene set enrichment analysis: a knowledge-based approach for interpreting genome-wide expression profiles. *Proc Natl Acad Sci U S A* **102**, 15545-15550, doi:10.1073/pnas.0506580102 (2005).

76. Franke, D., Harris, D. K., Xie, L., Jensen, K. F. & Bawendi, M. G. The Unexpected Influence of Precursor Conversion Rate in the Synthesis of III-V Quantum Dots. *Angew Chem Int Ed Engl* **54**, 14299-14303, doi:10.1002/anie.201505972 (2015).

77. Franke, D. *et al.* Continuous injection synthesis of indium arsenide quantum dots emissive in the short-wavelength infrared. *Nat Commun* **7**, 12749, doi:10.1038/ncomms12749 (2016).

78. Bruns, O. T. *et al.* Real-time magnetic resonance imaging and quantification of lipoprotein metabolism in vivo using nanocrystals. *Nat Nanotechnol* **4**, 193-201, doi:10.1038/nnano.2008.405 (2009).